The First Extrasolar Planet Discovered with a New Generation High Throughput Doppler Instrument

Jian Ge[1], Julian van Eyken[1,2], Suvrath Mahadevan[1,2], Curtis DeWitt[1], Stephen R. Kane[1], Roger Cohen[1], Andrew Vanden Heuvel[1], Scott W. Fleming[1] & Pengcheng Guo[1]

Department of Astronomy, The University of Florida, Gainesville, FL 32611

Gregory W. Henry

Center of Excellence in Information System, Tennessee State University, 3500 John A. Merritt Blvd., Box 9501, Nashville, TN 37209

Donald P. Schneider & Lawrence W. Ramsey

Department of Astronomy & Astrophysics, The Pennsylvania State University, University Park, PA 16802

Robert A. Wittenmyer, Michael Endl & William D. Cochran

Department of Astronomy, The University of Texas, Austin, TX 78712

Eric B. Ford

Department of Astronomy, The University of California, Berkeley, CA 94720

Eduardo L. Martín, & Garik Israelian

Instituto de Astrofisica de Canarias, La Laguna (Tenerife), Spain

Jeff Valenti

Space Telescope Science Institute, 3700 San Martin Drive, Baltimore, MD 21218

and

David Montes

Departamento de Astrofísica y Ciencias de la Atmósfera, Facultad de Físicas, Universidad Complutense de Madrid, E-28040 Madrid, Spain

jge@astro.ufl.edu

[1]Visiting Astronomer, Kitt Peak National Observatory. KPNO is operated by AURA, Inc. under contract to the National Science Foundation.

[2]Michelson Graduate Fellow

ABSTRACT

We report the detection of the first extrasolar planet, ET-1 (HD 102195b), using the Exoplanet Tracker (ET), a new generation Doppler instrument. The planet orbits HD 102195, a young star with solar metallicity that may be part of the local association. The planet imparts radial velocity variability to the star with a semiamplitude of 63.4 ± 2.0 m s^{-1} and a period of 4.11 days. The planetary minimum mass ($m \sin i$) is 0.488 ± 0.015 M_J.

The planet was initially detected in the spring of 2005 with the Kitt Peak National Observatory (KPNO) 0.9 m coudé feed telescope. The detection was confirmed by radial velocity observations with the ET at the KPNO 2.1 m telescope and also at the 9 m Hobby-Eberly Telescope (HET) with its High Resolution Spectrograph. This planetary discovery with a 0.9 m telescope around a $V = 8.05$ magnitude star was made possible by the high throughput of the instrument: 49% measured from the fiber output to the detector. The ET's interferometer-based approach is an effective method for planet detection. In addition, the ET concept is adaptable to multiple-object Doppler observations or very high precision observations with a cross-dispersed echelle spectrograph to separate stellar fringes over a broad wavelength band.

In addition to spectroscopic observations of HD 102195, we obtained brightness measurements with one of the automated photometric telescopes (APTs) at Fairborn Observatory. Those observations reveal that HD 102195 is a spotted variable star with an amplitude of ~ 0.015 mag and a 12.3 ± 0.3 day period. This is consistent with spectroscopically observed Ca II H and K emission levels and line broadening measurements but inconsistent with rotational modulation of surface activity as the cause of the radial velocity variability. Our photometric observations rule out transits of the planetary companion.

Subject headings: instrumentation: interferometers — instrumentation: spectrographs — planetary systems — stars: individual (HD 102195) — techniques: radial velocities

1. Introduction

Over the past fifteen years, the field of extrasolar planets has moved from the fringes of science to become a central pillar of current and future astronomical studies. Although the first extrasolar planets were discovered by radio observations of a pulsar (Wolszczan &

Frail 1992), the vast majority of the over 170 known extrasolar planets orbit main sequence stars and were found using cross-dispersed echelle spectrographs at a dozen ground-based telescopes. The first detected extrasolar planet associated with a main sequence star, 51 Peg (Mayor & Queloz 1995), ushered in a continuous stream of unexpected results on extrasolar planets, ranging from their extreme diversity ("hot Jupiters", planets in very elongated orbits, multiple-Jupiter-mass planetary systems) to the recently discovered super-Earth-mass planets around solar-type stars with orbital periods of a few days. A review of the field is given by Marcy et al. (2005). These discoveries not only provide new challenges for the fields of planetary origins and evolution, but also indicate that a large sample of planets is required to obtain a full understanding of their nature.

Although the high-precision echelle Doppler instruments have proven quite successful at detecting extrasolar planets, the current approach is costly and time-consuming because of the large telescopes required and the relatively low throughputs (a few percent) of the spectrographs as well as the limitation of observing one star at a time. A sample of approximately 5,000 stars (generally the closest and brightest ones), including the 2000 N2K survey stars targeting for short period planets (Fischer et al. 2005), has been monitored for planets with echelle instruments on a dozen telescopes, including most of the new generation large telescopes such as the Keck, the Very Large Telescope (VLT), Subaru, the Hobby-Eberly Telescope (HET), and Magellan. Most of the target stars have visual magnitudes brighter than about 8.0 except the N2K targets stars with visual magnitudes brighter than about 10.5 (Fischer et al. 2005). Based on the current planetary detection rate of $\sim$ 7% among solar type stars (Marcy et al. 2005), a few hundred planets will likely be detected over the next ten years using current techniques. Given the surprising range of properties known to date (and the likelihood of even larger surprises in the future), this sample will still be inadequate for giving us a comprehensive picture of planet formation and evolution and their relation to stellar properties such as mass, luminosity, spectral type, metallicity, duplicity, and age. Furthermore, to monitor a large number of stars, one must move to targets with $V > 8.0$. An instrument with high throughput becomes critical to search for planets around fainter stars. In addition, an instrument with multiple object capability would greatly enhance the efficiency of any extrasolar planet survey.

A promising Doppler technique for finding extrasolar planets, one that is quite different from the echelle approach, uses a dispersed fixed-delay interferometer (DFDI) for precision radial velocity measurements. The DFDI offers high throughput and multi-object capability. Instead of measuring the absorption line centroid shifts in the echelle approach, a DFDI determines the radial velocity by monitoring interference fringe phase shifts. The idea for using a fixed-delay interferometer for high precision Doppler measurements was first proposed by solar astrophysicists in the 1970s and 1980s to measure solar oscillations (Barker &

Hollenbach 1972; Gorskii & Lebedev 1977; Beckers & Brown 1978, Kozhevatov 1983). This approach was adopted by the Global Oscillations Network Group (GONG) interferometer (Harvey et al. 1995). The GONG interferometer, with a narrow passband ($\sim$ 1 Å), has produced very high Doppler precision measurements of the sun (sub m s^{-1} precision for the GONG measurements; Harvey 2002, private communication). The concept of combining a fixed-delay interferometer with a moderate resolution spectrometer for broad band operations for high precision stellar Doppler measurements was proposed in 1997 by David Erskine at Lawrence Livermore National Lab. The initial lab experiments and telescope observations successfully demonstrated the DFDI concept [earlier this concept was called fringing spectrometer and Externally Dispersed Interferometer (EDI), Erskine & Ge 2000; Ge, Erskine & Rushford 2002]. The theory for DFDI is described in Ge (2002). In 2002 a prototype DFDI instrument, designated as the Exoplanet Tracker (ET), was used at the KPNO 2.1 m telescope to reproduce the radial velocity curve of the known planet orbiting the solar type star 51 Peg (van Eyken et al. 2004a), demonstrating the capability of this new approach for planet detection. A new version of the ET instrument, optimized for high throughput and relatively large wavelength coverage compared to the 2002 prototype, was commissioned at the KPNO 0.9 m coudé feed and 2.1 m telescopes in 2003 November (Ge et al. 2004; van Eyken et al. 2004b). The first DFDI multi-object observations, using a modified ET, were obtained in 2005 March at the 2.5 m Sloan Digital Sky Survey (SDSS) telescope (York et al. 2000; Gunn et al. 2006) at Apache Point Observatory (Ge et al. 2005).

In this paper, we report the first detection of a new extrasolar planet using the DFDI technique. The planet, HD 102195b (ET-1), associated with the star HD 102195, has an orbital period of 4.11 days and was discovered with ET at the KPNO 0.9 m coudé feed and 2.1 m telescopes. The planet survey instrumentation and observations are reviewed in section 2, and a description of the survey data processing is provided in section 3. Section 4 presents additional radial velocity, spectroscopic, and photometric observations of HD 102195. An analysis of the radial velocity curve and follow-up data of HD 102195 and a brief discussion of the properties of ET-1 are given in sections 5 and 6, respectively.

2. Exoplanet Tracker: Description and Initial Survey

In the winter of 2004 we began a small-scale extrasolar planet survey at KPNO using the DFDI approach. This program is designed to detect new planets with short orbital periods (< 10 days). Targets were chosen primarily from the Nstar catalogue (Gray et al. 2003), selecting dwarf stars of type FGK with $7.8 < V < 9$. Stars that were known to be fast rotators or had high activity indicators were removed from the sample, as were any

known visual doubles or variables. Since studies have shown a strong correlation between frequency of planetary systems and high metallicity in the star (e.g., Gonzalez 1997; Reid 2002; Santos et al. 2004; Fischer & Valenti 2005), we selected relatively high metallicity stars ([M/H]>0.0.) to increase the planet detection efficiency.

Below we present a brief outline of the DFDI instrument, ET, of which a more detailed description can be found in van Eyken et al (2004b). ET includes a single object fiber feed system, a Michelson type interferometer with a fixed optical delay in one of the arms, a spectrograph with a Volume Phase Holographic (VPH) grating, and a 4k×4k CCD camera with 15 μm pixels. An optical fiber with a 200 μm core diameter (2.5″ on the sky) is fed by an $f/8$ beam from the KPNO 0.9 m coudé feed or 2.1 m telescope (both telescopes are housed in the same enclosure and feed the same spectrograph, so the instrument does not have to be relocated). The fiber has an $f/6$ output beam. ET is designed to operate from 5000–5640 Å and has a spectral resolving power of ∼5,100. A resolution element is sampled by 6.7 pixels in the dispersion direction. Each fringe is sampled by $\sim$ 58 pixels in the slit direction; this range usually includes $\sim$ 5 periods of fringing. The VPH grating is a Dickson type design, which produces a 92% peak grating efficiency but with a limited grating operation band of $\sim$ 600 Å. The CCD camera was purchased from Spectral Instrument Inc. The detector is a back-illuminated CCD with $\sim$ 90% quantum efficiency in the ET operating wavelengths.

The measured instrument throughput from the fiber output to the detector is 49%. The overall average detection efficiency, including the telescope, seeing, fiber, instrument and detection losses, is 18% under typical seeing conditions ($\sim$ 1.5″) at the KPNO coudé feed/2.1 m. An iodine vapor glass cell 150 mm long and 50 mm in diameter is used as a Doppler zero-velocity reference. The cell temperature is stabilized to 60 ± 0.1°C. Since 2003, we have been able to recover the expected RV signatures of known planets routinely with the ET instrument (see Figure 1) and have obtained short term (two day) precision as high as 3.6 m s^{-1} (photon noise limited) on the bright RV stable star 36 UMa (van Eyken et al. 2004b). The instrument long term precision has not been well chacterized yet. The preliminary RV measurements over two months show that the instrument is at least stable to $\sim$ 13 m s^{-1}.

The initial ET planet survey of 90 stars without previous precision radial velocity observations was conducted during the period 2004 December–2005 May with the KPNO 0.9 m coudé feed from December to March and the 2.1-m telescope in May. A total of 59 nights of the coudé feed time and 7 nights of 2.1-m time were allocated to the program. Observations on 43 nights were obtained during the survey (losses were primarily due to poor weather).

The survey was divided into five observation blocks, each of $\sim$ 10 nights duration. Star and iodine templates were obtained at the beginning and end of each block (van Eyken et

al. 2004a). For a typical block, 5–6 RV measurements were acquired for each survey star. The RV data were taken with the iodine vapor cell in the stellar beam. The instrument was set to the same configuration during each observation block to maximize the instrument stability. The interferometer fringe pattern was stablized by a closed-loop, actively-controlled piezoelectric transducer (PZT) system connected to one of the interferometer arms. The fringe pattern was monitored with a stablized HeNe laser at 0.6328 μm purchased from Melles Griot Inc. To measure the illumination profile and the spectral line slant for each fringe while maximizing the instrument stability, the interferometer fringes were jittered at the beginning and the end of each observation block to produce non-fringe calibration data. The jitter of the interferometer fringes was produced by operating the interferometer PZT ramp generators at about 10 Hz. The interferometer phase was locked during the observations in each block. The instrument room was heated to ∼24°C, and the rms temperature fluctuation during the runs was approximately 0.1°C. The absolute velocity drift due to the temperature fluctuation and mechanical instability is about 1–2 km s^{-1}. This velocity drift is calibrated and corrected with the iodine absorption line fringes.

Typical individual exposure times are ∼25 min for $V \sim 8$ and ∼40 min for $V \sim 9$ stars at the coudé feed; typical exposure times for the 2.1 m are 10 min for all targets. The average rms RV precision (photon noise) is ~ 20 m s^{-1} at the coudé feed and ~ 17 m s^{-1} at the 2.1 m. A total of ∼650 ET observations of 90 stars were obtained during this campaign.

3. Survey Data Processing

The data produced by ET required the development of a large software processing system. In this section we briefly outline the steps required to extract precision RV measurements from the raw data recorded by the detector. The main steps in the processing of the ET fringe spectra are (1) image pre-processing, (2) sinusoid fitting, and (3) RV shift determination.

Preprocessing: Image preprocessing is performed with a combination of standard IRAF procedures[1] and proprietary software written in Research Systems Inc's IDL data analysis language. The steps consist of the following:

Background subtraction/trimming: Detector bias and background light calibration images (dark plus stray light) are first subtracted from the raw data. An attempt is made to remove

[1]IRAF is distributed by the National Optical Observatory, which is operated by the Association of Universities for Research in Astronomy, Inc., under contract with the National Science Foundation.

as much internally scattered light as possible by fitting a smooth function to the dark areas of the images and using a one-dimensional interpolation scheme to estimate the scattered light levels in the areas covered by the spectra. The two-dimensional frames are then trimmed into new two-dimensional frames including only fringe spectra.

Flatfielding: Pixel-to-pixel sensitivity variations are corrected by dividing the data by a flatfield calibration image taken with a tungsten lamp. The irregular illumination of the spectrum is repaired by the application of a 'self illumination correction' algorithm. This process constructs a second flatfield by extracting the underlying illumination function from each individual image (see van Eyken et al. 2004a).

Slant correction: An algorithm is applied to correct for misalignment of the spectral lines with the rows/columns of the CCD. This feature is caused by a combination of imperfect alignment of the CCD and by aberration and distortion in the instrument optics (i.e., a simple rotation will not correct the alignment over the entire detector). This step is essential to obtain the proper cuts along the wavelength channels required to obtain uniform fringes.

Low pass filtering: Finally, a one-dimensional, low-pass Fourier filter is applied to the data in the dispersion direction. This action removes the interferometer comb, the pattern of parallel lines that is created by the continuum and therefore contains no Doppler information.

Phase and Visibility Determination: Once the initial image processing is complete, the phases and visibilities of each wavelength channel (column) are measured. This is achieved simply by fitting a sine wave to each wavelength channel in the image with a standard χ^2 minimization algorithm. The fit is weighted according to the number of counts in the original non-flatfielded data, on the assumption of photon noise dominated error.

To determine the phase accurately, two passes of the curve-fitting are performed to determine the fringe frequency. The first pass determines the frequencies of each channel. A polynomial is then fit to the frequencies as a function of wavelength (weighted according to the measurement errors). The process is repeated a second time but with the frequencies fixed to match this function. This approach was found to significantly improve the final precision.

Determining the Intrinsic Doppler Shift: Once the phase and visibility values are obtained for all wavelength channels, we combine them to form a vector vs. wavelength channel called a whirl, where each vector represents the fringe amplitude and phase (see the definition in Erskine & Ge 2000). In general, the star+iodine data whirl will be a linear vector combination of the iodine and star template whirls, where the template whirls are rotated in phase by an amount that must be determined. A set of four simultaneous linear equations can be constructed for each pair of channels (Erskine 2003). The solution for the

phase rotations is found by linearizing the complete overdetermined set of equations across all channels and using singular value decomposition. This procedure returns a "best fit solution" along with standard error estimates. The measured rotations correspond to the star shift and the intrinsic instrument shift. The difference between these two rotations yield the intrinsic stellar RV shift.

In addition to the two phase rotations, several additional degrees of freedom are allowed in our processing. In particular, we allow for bulk shift of the entire spectrum in the dispersion direction. This change can be produced by a Doppler shift or by movement of the CCD detector due to thermal flexure. This, along with additional flexures in the instrument optics, can create translations of the image. A reduced χ^2 value is determined between the star+iodine data and the best superposition of the pixel-shifted and rotated templates. This process is iterated until a minimum is reached in the reduced χ^2.

After correcting for instrument drift, it still remains to apply a barycentric correction to the velocities to account for the motion of the Earth. This is done using our own software written in IDL. Diurnal motion is corrected using an algorithm adapted from the IRAF procedure 'rvcorrect' in the NOAO package. Annual motion is corrected using the 'baryvel' routine from the IDL astronomy library (ref. http://idlastro.gsfc.nasa.gov), which is based on the algorithm from Stumpff (1980).

At the completion of the data processing, the 90 stars in the survey fell into three catagories: (1) 75 of the stars exhibited less than 2.5σ RV scatter about a mean value; (2) 10 stars had RV variations between 2.5σ and 1000 m s^{-1} rms about the mean; and (3) 5 stars were spectroscopic binaries with RV variations larger than 1000 m s^{-1} rms. Only stars in the second group were considered candidates for harboring a planet and, of those ten stars, HD 102195 appeared to be the most promising candidate.

4. HD 102195

Having identified HD 102195 as the most promising planetary-candidate star from our initial Exoplanet Tracker survey, we embarked on a series of additional observations of HD 102195 to determine the nature of the RV variations. We obtained further precision RV measurements as well as high-resolution spectroscopy, Ca II H and K emission-line spectroscopy, and high-precision photometry.

4.1. Additional Radial Velocities

The initial 14 coudé measurements of HD 102195 with the ET had an rms variation of slightly more than 60 m s^{-1}, with typical single-measurement errors of 20 m s^{-1}. An additional 14 ET measurements were made in 2005 May with the KPNO 2.1 m telescope and the same ET instrument. Figure 2 displays all 28 spring 2005 ET radial velocities of the star and confirms HD 102195 as a good planetary candidate host star.

The KPNO 2.1 m ET system was used again in 2005 December to obtain an additional 21 RV measurements of HD 102195. We also acquired 10 RV measurements of the star between 2005 November and 2006 January with the High Resolution Spectrograph (HRS) of the Hobby-Eberly Telescope (HET) (Ramsey et al. 2006) to confirm the ET results. The HET/HRS data were obtained with a $2''$ fiber and exposure times of 10 minutes. These observations were conducted with the HRS $R = 60,000$ cross-dispersed echelle mode. This is the standard HRS configuration for precision RV measurements, and the data were processed with the techniques described in Cochran et al. (2004). The HET observations, which have typical internal errors of $\sim$2 m s^{-1}, were able to be timed for maximum phase leverage because of the queue-scheduled operation of the telescope. All 59 precision RV measurements of HD 102195 from all sources are presented in Table 1.

4.2. High-Resolution Spectra

A total of nine high-resolution ($R = 150,000$) spectra of HD 102195 were obtained with the SARG spectrograph on the 3.5 m TNG telescope at La Palma on 2005 June 19, 20, and 21. The wavelength coverage is complete from 3700 Å to 10000 Å. These data were used to monitor line-bisector variations, to determine stellar properties (metallicity, $\log g$, $T_{\rm eff}$ and $v \sin i$), and to search for any evidence of a second set of lines in the system. The SARG spectra were processed through a data pipeline developed by J. Valenti for the N2K Consortium short-period planet survey (Valenti & Fischer 2005). Figure 3 shows a section of the SARG data centered at a wavelength of 6140 Å. The typical signal-to-noise ratio (S/N) for each spectrum is about 100 per pixel. The nine spectra were normalized and fitted with synthetic spectra to derive the stellar parameters. The average values of the derived parameters are reported in section 5.1. The nine spectra were searched for line bisector variations, but no significant variations were found over the three days. For instance, the average bisector velocity span for each day is -1.9 ± 12.4 ms^{-1}, 5.2 ± 12.0 ms^{-1}, and 23.6 ± 11.7 ms^{-1} for June 19, 20 and 21, respectively. Details on the line bisector analysis can be seen in Martinez Fiorenzano et al. (2005). ,

In addition, one high resolution spectrum of HD 102195 was obtained with the 2.2 m telescope at the German Spanish Astronomical Observatory (CAHA) (Almería, Spain) on 2006 January 14. The Fibre Optics Cassegrain Echelle Spectrograph (FOCES) (Pfeiffer et al. 1998) was used with a 2048 × 2048 24μm SITE#1d15 CCD detector. The wavelength range covers from 3500 to 10700 Å in 111 orders. The reciprocal dispersion ranges from 0.04 to 0.13 Å/pixel and the spectral resolution, determined as the full width at half maximum (FWHM) of the arc comparison lines, ranges from 0.08 to 0.35 Å. A signal to noise ratio S/N=100 per pixel was obtained in the Hα line region.

The spectra have been extracted using the standard reduction procedures in the IRAF package (bias subtraction, flat-field division and optimal extraction of the spectra). The wavelength calibration was obtained by taking spectra of a Th-Ar lamp. Finally, the spectra have been normalized by a polynomial fit to the observed continuum.

This spectrum was used to determine stellar properties, analyze the chromospheric activity, and estimate the age from the Lithium line (Li I 6707.8).

4.3. Ca II H and K Observations

HD 102195 was observed between 2005 December 14–20 with the KPNO 0.9 m coudé spectrograph to monitor the emission at the core of the Ca H and K lines. The observations were obtained with Grating A, Camera 5, the long collimator, a 400 μm slit, and a 2k×2k CCD camera. This configuration produced a spectral resolving power of 10,000 over a wavelength range of 230 Å centered on 4010 Å. A total of 29 spectra were obtained during the run. The spectra were processed with standard IRAF procedures. A reference star, τ Ceti, was monitored for comparison. Emission is clearly seen in the core of the Ca II H and K lines (see Figure 4), as expected by the classification of this star as mildly active by Strassmeier et al. (2000).

4.4. High-Precision Photometry

Between 2005 April and 2006 February, we obtained high-precision photometry of HD 102195 with the T10 0.8 m automatic photometric telescope (APT) at Fairborn Observatory. These observations covered the last part of the 2004–05 and the first part of the 2005–06 observing seasons. The APTs can detect short-term, low-amplitude brightness variability in the stars caused by rotational modulation in the visibility of magnetic surface features such as spots and plages (e.g., Henry, Fekel, & Hall 1995) as well as longer-term

variations associated with stellar magnetic cycles (Henry 1999). Thus, photometric observations can help to establish whether observed radial velocity variations are caused by stellar activity or planetary-reflex motion (e.g., Henry et al. (2000a). Queloz et al. (2001) and Paulson et al. (2004) have found several examples of periodic radial velocity variations in solar-type stars caused by photospheric spots and plages. The APT observations are also useful to search for possible transits of the planetary companions (Henry et al. 2000b; Sato et al. 2005).

The T10 APT is equipped with a two-channel precision photometer containing two EMI 9124QB bi-alkali photomultiplier tubes to make simultaneous measurements in the Strömgren b and y passbands. The APT measures the difference in brightness between a program star and one or more nearby comparison stars. The primary comparison star used for HD 102195 was HD 102747 ($V = 7.77$, $B - V = 0.513$, F5); a secondary comparison star was HD 101730 ($V = 6.94$, $B-V = 0.49$, F5). Strömgren b and y differential magnitudes were computed and corrected for differential extinction with nightly extinction coefficients and transformed to the Strömgren system with yearly mean transformation coefficients. Finally, we combined the Strömgren b and y differential magnitudes into a single $(b + y)/2$ passband to maximize the precision of the photometric measurements. The typical external precision of the differential magnitudes is 0.0012–0.0016 mag for this telescope, as determined from observations of pairs of constant stars. The standard deviation of our comparison star 2 minus comparison star 1 differential magnitudes is 0.0019, close to the typical precision and indicating very little variability in either comparison star. However, the HD 102195 minus comparison star 1 differential magnitudes have standard deviations of 0.0048 and 0.0033 mag in observing seasons 1 and 2, respectively, indicating clear variability in HD 102195. The 468 individual differential magnitudes of HD 102195 minus the primary comparison star are given in Table 2. Further information on the automatic telescope, photometer, observing procedures, and data reduction techniques can be found in Henry (1999) and Eaton, Henry, & Fekel (2003).

5. Results

5.1. Stellar Properties

HD 102195 was identified as a K0V star with a color of $(B-V) = +0.84$ (Strassmeier et al. 2000). The *Hipparcos* parallax (ESA 1997) of 34.51±1.16 mas places this target at 29 pc. The apparent visible magnitude is $V = 8.05 \pm 0.03$ measured from the APT photometry. The absolute magnitude is $M_V = 5.73$. Montes et al. (2001) suggest that HD 102195 may belong to the Local Association, which, if confirmed, would place the age of the star at 20–

150 Myr. Following the procedure described in Valenti & Fischer (2005), our spectroscopic analysis of the SARG spectra ($R \sim 150,000$) yields $T_{\rm eff} = 5330 \pm 28$K, [Fe/H]= 0.096±0.032, $\log g = 4.368 \pm 0.038$ [log(cm s^{-2})], and $v \sin i = 3.23 \pm 0.07$ km s^{-1}. The fit of this model to the combined spectrum is shown in Figure 3. The effective temperature and surface gravity of the star appears to be consistent with a G8V.

We interpolated the "high temperature" table of VandenBerg & Clem (2003) as a function of spectroscopic effective temperature, gravity, and iron abundance to obtain a V-band bolometric correction of -0.177. Applying this correction to the observed V-band magnitude of 8.05 ± 0.03 yielded a stellar luminosity of 0.463 ± 0.034 L$_\odot$.

We used our spectroscopically determined [Ti/Fe] abundance ratio as a crude measure of α-element enrichment, obtaining 0.049 ± 0.042. We detect no significant α-element enhancement, but for consistency with Valenti & Fischer (2005), we used our measured α-element enhancement of 0.049 when interpolating the Y^2 isochrones, slightly perturbing our derived stellar properties.

We used the stellar luminosity and the spectroscopic effective temperature, iron abundance, and α-element enrichment to interpolate the Y^2 isochrones (Demarque et al. 2004), obtaining a stellar mass of 0.926 $M_\odot$ and a stellar radius of 0.835 R$_\odot$. In addition, the most probable age is 2.0 Gyr with an asymmetric 1σ confidence interval spanning the range 0.6 to 4.2 Gyr. This age estimate is much older than that derived from the Local Association by Montes et al. (2001). The chromospheric activity of HD 102195 has been measured by Strassmeier et al. (2000). The chromospheric emission ratio, $\log R'_{HK} = -4.30$, indicates this is a mildly active star (Noyes et al. 1984). The stellar parameters are summarized in Table 3.

Further analysis of the FOCES high resolution optical spectrum of HD 102195 was conducted to independently derive the stellar properties. Here we summarize the results.

Spectral Type

To obtain an independent estimate of the spectral type of this star, we have compared the spectrum of HD 102195 with that of inactive reference stars taken during the same observing run. The analysis makes use of the program STARMOD developed at Penn State University (Barden 1985) and modified more recently by us. With this program a synthetic stellar spectrum is constructed from the artificially rotationally broadened, and radial-velocity shifted spectrum of an appropriate reference star. We obtained the best fit between observed and synthetic spectra when we use a G8-dwarf spectral type standard star (HD 182488). The uncertainty in this classification is of one spectral subtype as is typical in the MK spectral classification. The careful analysis of the wings of the Hα and Na I D$_1$ and D$_2$ lines clearly

indicates a better fit with a G8V than with a K0V. This spectral classification agrees with the results of the spectral synthesis of the SARG spectra.

Rotational velocity

By using the program STARMOD we have obtained the best fits with $v \sin i$ values between 3 and 4 km s^{-1}. In order to determine a more accurate rotational velocity of this star we have made use of the cross-correlation technique by using the routine FXCOR in IRAF. When a stellar spectrum with rotationally broadened lines is cross-correlated against a narrow-lined spectrum, the width of the cross-correlation function (CCF) is sensitive to the amount of rotational broadening of the first spectrum. Thus, by measuring this width, one can obtain a measurement of the rotational velocity of the star. The observed spectrum was $cross - correlated$ against the spectrum of a template star (the G8V star HD 182488) and the width (FWHM) of CCF determined. The rotational velocity of HD 182488 is 0.6 ± 0.5 km/s, this values has been determined by Fekel (1997) by a method based in the determination of the intrinsic stellar broadening from the observed FWHM of weak or moderate-strength lines, corrected from instrumental profile and from macroturbulent broadening. The calibration of this width to yield an estimation of $v \sin i$ is determined by cross-correlating artificially broadened spectra of the template star with the original template star spectrum. The broadened spectra was created for $v \sin i$ spanning the expected range of values by convolution with a theoretical rotational profile (Gray 1992) using the program STARMOD. The resultant relationship between $v \sin i$ and FWHM of the CCF was fitted with a fourth-order polynomial. The $v \sin i$ obtained in this way for HD 102195 is 3.7±0.6 km s^{-1} which is in good agreement with the value derived from the SARG spectra.

Radial velocity

The previous known value of the heliocentric radial velocity of this star is 2.1±0.6 km s^{-1}, a weighted mean value of the two measurements reported by Strassmeier et al. (2000).

In the FOCES spectrum the heliocentric radial velocity has been determined by using the cross-correlation technique. The spectrum of HD 102195 was cross-correlated order by order, by using the routine FXCOR in IRAF, against the spectrum of the K0V radial velocity standard HD 3651 (Barnes et al. 1986). We have used the K0V star HD 3651 because the G8V star HD 182488 was not observed in the same observing run as that for HD 102195. However, we have determined also the radial velocity using HD 182488 and the result is very similar. The radial velocity was derived for each order from the peak of the cross-correlation function peak (CCF), and the uncertainties were calculated by FXCOR based on the fitted peak height and the antisymmetric noise as described by Tonry & Davis (1979). Those orders which contain chromospheric features and prominent telluric lines have been excluded when

determining the mean velocity. The resulting value is $V_{\rm hel}$ = 2.04±0.07 km s^{-1}.

Kinematics and age

The galactic space-velocity components (U, V, W) have been determined by Montes et al. (2001) using heliocentric radial velocity of 2.1±0.6 km s^{-1} (Strassmeier et al. 2000) and the precise proper motions taken from Hipparcos (ESA 1997) and Tycho-2 (Høg et al. 2000) catalogues. Solely on the basis of kinematics criteria Montes et al. (2001) classified HD 102195 as a young disk star and a possible member of the Local Association moving group. The age of this complex moving group is in the range of 20 to 150 Myr; however, the age inferred from the Lithium line strength does not agree with such a young age.

As it is well known, the Li I line at λ6708 Å is an important diagnostic of age in late-type stars, since it is destroyed easily by thermonuclear reactions in the stellar interior (e.g. Soderblom et al. 1990). In the FOCES spectrum a small absorption Li I line is observed blended with the nearby Fe I λ6707.41 Å line. We have corrected the total measured equivalent width, EW(Li I+Fe I) = 17.4 mÅ, by subtracting the EW of Fe I calculated from the empirical relationship with (B–V) given by Soderblom et al. (1993). Very similar results are also obtained using the espiral relationship given by Favata et al. (1993). The resulting corrected EW(Li I) is 2.8 mÅ, in agreement with the value previously reported by Strassmeier et al. (2000) of 3 mÅ.

Comparing the EW(Li I) of HD 102195 with those of well-known young open clusters of different ages in a EW(Li I) versus spectral type diagram (Montes et al. 2001 and references therein), a much greter age than the Local Association is inferred, it could be even older than the Hyades. This result and the relatively low level of chromospheric activity (see below) favor the range of age deduced from the Y2 isochrones.

Chromospheric activity indicators

The FOCES 01/14/06 echelle spectrum of HD 102195 allows us to study the behaviour of the different chromospheric activity indicators from the Ca II H & K to the Ca II IRT lines, which are formed at different atmospheric heights. The chromospheric contribution in these features has been determined by using the spectral subtraction technique (see Montes et al. 2000). The spectral subtraction technique is the subtraction of a synthesized stellar spectrum constructed from artificially rotationally broadened, and radial velocity shifted spectrum of an inactive star chosen to match the spectral type and luminosity class of the active star under consideration. The synthesized spectrum was constructed using a G8V reference star with the program STARMOD.

In the observed spectrum only the Ca II H & K lines are clearly detected in emission.

After applying the spectral subtraction a small excess chromospheric emission is detected in the Hα and Ca II IRT (λ8498, λ8542, λ8662) lines. However, the other Balmer lines as well as the Na I D_1 and D_2 lines do not show evidences of filled-in absorption by chromospheric emission.

In Table 4 we give the excess emission equivalent width (EW) (measured in the subtracted spectra) for the Ca II H & K, Hα and Ca II IRT lines and the corresponding absolute chromospheric flux at the stellar surface (logF_S (erg cm^{-2} s^{-1})) obtained by using the calibration of Hall (1996) as a function of (B–V). For instance, the calibration of Hall (1996) give the flux in the continuum at the wavelengths 3950 Å (for the H&K CaII lines), 6563 Å (H_alpha line) and 8520 Å (CaII IRT lines) as a function of B-V. Using this flux in the continuum we convert the EW into logFs. The uncertainties in the measured EW were estimated to be in the range 10-20% taking into account: a) the typical internal precisions of STARMOD, b) the rms obtained in the fit between observed and synthesized spectra in the spectral regions outside the chromospheric features and c) the standard deviations resulting in the EW measurements.

The chromospheric activity index (R'_{HK}) obtained from the stellar surface in the Ca II H & K lines (which is corrected from the photospheric contribution by using the spectral subtraction) is log$R'_{HK} = -4.45$ similar to the value or -4.3 reported by Strassmeier et al. (2000).

It is well known the chromospheric activity is related to both the spectral type and rotational velocity. Late spectral type main sequence stars have larger chromospheric emission than early stars and as the star ages, it slows down its rotation and decrease the level of activity. In this sense the chromospheric activity provides an indication of the stellar age for a given spectral type. Using the calibration of Soderblom et al. (1991) for the chromospheric activity (measured by R'_{HK}) – age relation an age of 0.8 Gyr is inferred. This age is only an estimation, since these kind of calibration are strictly valid for chromospherically quiet stars (logR'_{HK} < -4.75) (see Saffe et al. 2005 for a discussion), but agrees with the age deduced from the Li I line and it is in the range of age deduced from the Y2 isochrones.

5.2. RV Analysis and Orbital Solution

The RV precision and stability of ET have been determined using the RV stable stars in our survey. We define RV stable stars (at our precision level) to be those stars that show a reduced $\chi^2 < 2$ to the fit of a constant RV value over the period of observation (typically $\sim$ 10 days). At the 0.9 m coudé during a typical observing block, 7 out of 15 search stars

satisfied this criterion. For those, we found a rms scatter of 18.9 m s^{-1} at a mean visual magnitude of 8.26 and typical exposure times of 20–30 min. Using the same criterion for the 2.1 m observations, we found 12 out of 24 stars to be RV stable. These stable stars had a mean standard deviation of 17.6 m s^{-1} about a constant RV. For the 2.1 m targets, which had $< V > = 8.48$, the typical exposure times were 10 minutes. For both configurations, the errors are consistent with the expected photon noise limit. For an independent check of the instrument, we were able to recover the RV curve for 51 Peg. Figure 1 shows the coudé feed results for 51 Peg with the predicted RV curve due to the 4.23-day companion 51 Peg b. The measured residual mean error (after the expected velocity induced by the planet) for the coudé feed observations of 51 Peg is 7.9 m s^{-1}, which is consistent with the photon noise limit.

A total of 59 radial velocities of HD 102195 have been obtained from 2005 January through 2006 January. In contrast with the stable stars, the velocity variability of HD 102195 is ~ 60 m s^{-1}, 3σ above the measurement noise for the ET measurements at the KPNO coudé, 6σ above the noise level of the ET measurements at the KPNO 2.1m, and approximately 30 times larger than the measurement noise for the HET/HRS measurements (see Table 1). A periodogram analysis was carried out with a RV fitting code running a combination of a Lomb-Scargle (L–S) periodogram (Lomb 1976; Scargle 1982) and an iterative grid-search algorithm to locate the best fit to the data. The interactive grid search is the method used to search parameter space for the best fitting model by adjusting model parameters until it converges on a solution. Figure 5 displays the L–S periodogram resulting from a Fourier analysis of the HD 102195 velocities. The horizontal dotted lines correspond to the false-alarm probabilities for a given L–S statistic (or power). A strong peak is found at a period of 4.11 days. The false alarm probability associated with this peak is $< 10^{-6}$.

We performed a Bayesian analysis of the RV data to identify if a planetary companion is present and determine their orbital parameters, following the methods in Ford (2005, 2006). The RV variations are modeled as a single planet on a circular orbit. We assume a prior $p(P, K, \phi, \vec{C}, \sigma_j) \sim [P(K + K_o)\sigma_j]^{-1}$, where P is the orbital period, K is the velocity semi-amplitude, ϕ is the orbital phase at the given epoch, C_i is the $i^{\rm th}$ constant velocity offset, and σ_j is the magnitude of the stellar jitter. We impose sharp cutoffs on the prior at $P_{\rm min} = 1$ day, $P_{\rm max} = 3$ year, $K_{\rm max} = 2$ km s^{-1}, $\sigma_{j,\rm min} = 1$ m s^{-1}, and $\sigma_{j,\rm max} = 1$ km s^{-1}. A modified Jeffery's prior is used for the velocity semi-amplitude to make the prior for K normalizable, and we choose a scale parameter of $K_o = 1$m s^{-1}. Our model also includes five velocity offsets, C_i, that are necessary due to the use of different velocity zero points for the various instruments and observing runs. We assume that each observation has an independent Gaussian observational uncertainty, $\sigma_{i,\rm obs}$, that is estimated from the photon statistics. We calculate the likelihood using an effective uncertainty of $\sigma_{i,\rm eff} = \sqrt{\sigma_{i,\rm obs}^2 + \sigma_j^2}$

for each observation. To calculate the posterior probability distribution function, we analytically integrate over all but two of the model parameters using the Laplace and WKB approximations. Then, we directly integrate over the two remaining model parameters, P and σ_j.

In Figure 6 we show the posterior probability density function (posterior PDF) marginalized over all model parameters except the orbital period, analyzing the observations from each observatory separately. The 14 observations with ET at the KPNO 0.9 m coudé feed have a significantly larger measurement uncertainty than the other observations and do not isolate a single orbital solution (upper middle panel). Based on these observations, we obtained 35 observations with the ET at the KPNO 2.1 m. Analysis of the velocities from the 2.1 m alone shows a $\geq 99.9\%$ posterior probability of having a periodic signal (compared with a constant velocity or quadratic trend), and a $\geq 99.3\%$ posterior probability integrated over all solutions contained in the peak at 4.1 days (lower middle panel). Based on early observations with the 2.1 m, we obtained ten additional very high precision radial velocity measurements using the echelle spectrograph on HET. The HET observations by themselves (bottom panel) display the same periodicity as found in the KPNO/ET observations. Combining all the radial velocity observations (top panel), we find that there is a single dominant peak at 4.11 days that we interpret as the result of perturbations by a $m \sin i \simeq 0.49 M_J$ planet.

In Figure 7, we show the marginalized posterior PDF combining all radial velocity observations. The posterior probability is dominated by one peak at $P = 4.11$ days that contains essentially all of the posterior probability. The peak near 1.3 days is a result of aliasing due to the day/night cycle and contains $\leq 10^{-9}$ of the posterior probability. The peak near 4.8 days shown in the coudé feed data (see inset) is the result of aliasing due to the lunar cycle (most observations occur near full moon) and contains only $\leq 10^{-18}$ of the posterior probability. Our best-fit solution has $P = 4.11453$ days, $K = 63.2$ m s^{-1}, $\sigma_j = 5.9$ m s^{-1}, and an rms of 16.0 m s^{-1}. We have also performed a Bayesian analysis using a full Keplerian model and the Markov chain Monte Carlo (MCMC) technique (Ford 2005). The present observations do not provide a significant detection of an orbital eccentricity, but do place upper limits on the allowed eccentricities. Marginalizing over all model parameters, we estimate that $\langle P \rangle \simeq 4.11434 \pm 0.00089$, $\langle K \rangle \simeq 63.4 \pm 2.0$m s^{-1} and $\langle \sigma_j \rangle \simeq 5.8 \pm 1.8$ m s^{-1}. Our MCMC simulations find a 5% posterior probability for all eccentricities larger than 0.096, and a 0.1% posterior probability for all eccentricities greater than 0.14. Table 5 summarizes the orbital parameters for HD 102195b.

An independent RV curve fitting was conducted using the *Gaussfit* software developed by part of the HST FGS science team (e.g., Jefferys et al. 1987; McArthur et al. 1994;

Cochran et al. 2004). This software uses a robust estimation method to find the combined orbital solution, where the offsets from different data sets are included as free parameters for fitting. Figure 8 shows the best-fit RV curve. The planet has a 4.1134±0.0009 day orbital period, which is consistent with the derived values from the L-S periodogram and also the Bayesian analysis. This analysis finds a solution with a minimum planet mass of 0.49 M_J in a nearly circular orbit with an eccentricity of 0.06±0.02. These values are in excellent agreement with the Bayesian analysis above. The semimajor axis has a minimum size of 0.049 AU.

The companion's mass is similar to other known hot-Jupiter exoplanets with similar orbital periods around solar-type stars. The low eccentricity is not surprising since tidal circularization is expected for such a close planetary companion.

5.3. Photometric Analysis

Plots of the T10 APT photometric measurements from the 2004–05 and 2005–06 observing seasons are shown in Figures 9 and 10, respectively. Although the observations from 2004–05 are relatively few (38), the photometric amplitude of HD 102195 was greater at that time. The top panel of Figure 9 clearly shows cyclic variability with an amplitude of around 0.015 mag. The power spectrum of these data is shown in the bottom panel of Figure 9 and gives a period of 12.3 ± 0.3 days, which we take to be the rotation period of the star made apparent by rotational modulation in the visibility of photospheric starspots. The lightcurve closely resembles those of other spotted stars (e.g., Henry, Fekel, & Hall 1995).

The top panel in Figure 10 plots all the photometric data for the 2005–06 observing season. A power spectrum of these second season observations exhibits the same 12.3-day periodicity but with much lower amplitude. The observations in this figure are plotted against planetary orbital phase computed from the orbital elements in Table 5; zero phase refers to a time of inferior conjunction (mid transit). A least-squares sine fit to the brightness measurements in the top panel gives a semi-amplitude of only 0.0004±0.0002 mag. Given the cycle-to-cycle variation in the lightcurve caused by a continually evolving starspot distribution, this small amplitude on the radial velocity period is consistent with *no* brightness variability on that period. Thus, the photometry supports planetary reflex motion as the cause of the radial velocity variability.

Since the 2005–06 brightness measurements are both more numerous and exhibit lower variability than the observations of the previous season, the observations from the second season are more suitable for seeking possible transits of the planet across the disk of the

star. The solid curve in each panel of Figure 10 approximates the predicted transit lightcurve, assuming a planetary orbital inclination of 90°(central transits). The out-of-transit light level corresponds to the mean brightness of the observations. The transit duration is estimated from the orbital elements, while the transit depth is derived from the estimated stellar radius (Table 3) and an assumed planetary radius equal to Jupiter's. The bottom panel of Figure 10 shows the observations around the predicted time of mid transit replotted with an expanded scale on the abscissa. The horizontal error bar below the predicted transit curve represents the estimated uncertainty in the time of mid transit, based on the orbital elements. The vertical error bar represents the 0.0019 mag precision of the observations.

These 2005–06 photometric observations of HD 102195 cover the predicted transit window quite well and reveal no sign of a transit. The 47 observations within the transit window in the bottom panel of Figure 10 have a mean brightness level of 0.3683 ± 0.0005 mag. The 383 observations outside the transit window have a mean of 0.3676 ± 0.0002 mag. Therefore, the mean brightness values inside and outside of the transit window agree to within 0.0007 mag, i.e., to within their respective uncertainties. Our photometric observations rule out even very shallow transit events.

6. Discussion

HD 102195 is a mildly active G8V dwarf. Stellar activity, such as starspots, introduces jitter into the RV measurements. The amplitude of the stellar jitter caused by stellar activity can be estimated from the previously derived formula of Santos et al. (2000). Using the measured chromospheric activity index, $R'_{HK} = 5 \times 10^{-5}$, we estimate that the RMS RV jitter should be ~ 19 m s^{-1}. This level is consistent with the estimate from the Bayesian analysis of the radial velocity observations. Based on previous RV studies of active G dwarfs with photometric variations similar to HD 102195 (e.g., Paulson et al. 2004; Santos et al. 2000), we expect that the semiamplitude of the starspot induced radial velocity variation for HD 102195 may be on the order of $\sim$ 10–20 m s^{-1}. Even if the photometric and RV periods were equal, the deduced level of stellar activity could not account for the observed RV variations in HD 102195. This strengthens the conclusion from §5.5 above that stellar activity is not responsible for the 4.11-day radial velocity variation.

It is unusual (and of some concern) that the 12.3-day photometric period appears to be exactly (at least within the measurement errors) three times that of the 4.11-day radial velocity period. Could three similar starspot groups spaced approximately 120° in longitude on the star be responsible for the observed radial velocity period? Figure 9 shows that there is essentially no power in the brightness variations at 4.11 days (corresponding to a

frequencey of 0.24 cycles per day). Conversely, an examination of Figure 7 shows that there is essentially no power in the radial velocity variations at the photometric period of 12.3 days. This mismatch of the photometric and radial velocity periods indicates that they arise from separate causes and supports the planetary interpretation.

The Ca II H and K emisison measurements also support the planetary interpretation of the RV variations in HD 102195. The standard technique for analyzing stellar H and K emission is the S index described by Duncan et al. (1991) This quantitiy is defined by Duncan et al. as S=(H+K)/(V+R) where V and R are the summed flux in un-normalized 20 Å wide continuum bands extending from 3891-3911 Å and 3991-4011 Å respectively and H and K are channels centered on the cores of the Ca II H and K and have a measured triangular instrument response of FWHM 1.09 Å. For our S index measurements using spectra obtained at the KPNO 0.9m coude' telescope we define the quantities V and R in the same way as Duncan et al. (1991) , but differ in our definition of the quantities H, K which we define as the integrated flux in 1.4 Å bands centered of the Ca II H and K lines. We call the resulting S index S_{coude} to differentiate it from the Mt Wilson S index. No attempt has been made to put S_{coude} on the Mt. Wilson scale, since we are only interested in the variability of S_{coude}. The analysis of the chromospheric activity traced by the S index does not show any variability at the 4.11 day period of the planet, but does display longer term changes that appear consistent with the photometric rotation period. The mean S_{coude} index for the entire run is measured to be 0.024, and varies from 0.023 to 0.025. For comparison, in the reference star, Tau Ceti, the S index measuremtn varies less than 0.0005. This result further suggests that stellar activity is not the source of the detected RV signals.

In addition, the stellar rotation period measured from the photometry is consistent with the projected rotation velocity measured from the spectral analysis of the SARG and FOCES high resolution spectra. The measured $v \sin i = 3.23 \pm 0.07$ km s^{-1} corresponds to a maximum rotation period of 13.1 ± 0.3 days if a stellar radius of 0.84 $R_\odot$ is adopted. This does indicate that the stellar rotation axis may be close to an inclination of 90°. However, as discussed in §5.5 above, photometric transits have been ruled out by our photometry.

This planetary detection is the first time an extrasolar planet has been discovered via RV variations around a star fainter than $V = 8$ with a sub-meter aperture telescope. This discovery was made possible by the high throughput of the ET instrument. The total measured system detection efficiency of 18% (from the telescope to the detector) or 49% (from the fiber output to the detector) is about four times higher than has been achieved with HARPS, a state-of-the-art echelle spectrograph being used on the ESO 3.6-m telescope (Pepe et al. 2002).

Future DFDI instruments promise additional capabilities. Due to the use of the single-

order medium resolution stellar spectra superimposed with interference fringes, this method can be easily modified to allow multiple-object Doppler measurements (Ge 2002). A prototype multi-object DFDI obtained data in the spring of 2005 with the SDSS telescope and demonstrated this feasibility (Ge et al. 2005).

In addition, for single-object observations, the single-order medium resolution spectrograph can be replaced with a cross-dispersed echellette spectrograph to cover multiple orders of dispersed fringes to gain wavelength coverage. The echellette can also increase the spectral resolution due to its higher dispersion over the low single-order blazed grating. Since the Doppler sensitivity is roughly proportional to the square root of the spectral resolution and wavelength coverage (Ge 2002), it is likely that an ET interferometer coupled with a cross-dispersed echellette will increase the Doppler sensitivity by a factor of $\sim$3–5 times over current designs.

In summary, the detection of a planet around HD 102195 with a DFDI instrument demonstrates that the new-generation, high-throughput interferometric Doppler method is an effective technique for identifying extrasolar planets. This approach offers a number of opportunities for high precision RV measurements and planet surveys, especially for stars fainter than previous surveys with echelle Doppler instruments have reached. This technique may become a significant component in the effort to assemble the large sample of extrasolar planets required for a comprehensive characterization of these objects.

We are grateful to Stuart Shaklan, Michael Shao, Chas Beichman, Richard Green, Skip Andree, Daryl Wilmarth, and the KPNO staff for their generous support and advice and to Larry Molnar for his help in the early photometric data acquisition. The HET observations, whose timings were critical, were made possible by the dedicated efforts of the HET staff. We are indebted to Sara Seager and Eric Agol for a number of stimulating discussions. We thank Aldo Martinez Fiorenzano for helping the line bisector analysis of HD 102195. We appreciate many valuable comments made by the referee, which helped to improve the paper quality. This work is supported by the National Science Foundation grant AST 02-43090, JPL, the Pennsylvania State University and the University of Florida. SM and JvE acknowledge the JPL Michelson Fellowship funded by NASA. GWH is greatful for the effors of Lou Boyd at Fairborn Observatory and acknowledges support from NASA grant NCC5-511 and NSF grant HRD 97-06268. E.B.F. acknowledges the support of the Miller Institute for Basic Research. WDC, ME, and RAW were supported by NASA grants NNG04G141G and NNG05G107G to The University of Texas at Austin. The Hobby-Eberly Telescope (HET) is a joint project of the University of Texas at Austin, the Pennsylvania State University, Stanford University, Ludwig-Maximillians-Universität München, and Georg-August-Universität Göttingen. The HET is named in honor of its principal benefactors, William P. Hobby and Robert E. Eberly.

DM was supported by the Universidad Complutense de Madrid and the Spanish Ministerio de Educación y Ciencia (MEC), Programa Nacional de Astronomía y Astrofísica under grant AYA2005-02750. DM is grateful to Raquel M. Martínez, Jesús Maldonado and Benjamín Montesinos for their help during the observations. FOCES high resolution optical spectra were based on observations collected at the Centro Astronómico Hispano Alemán (CAHA) at Calar Alto, operated jointly by the Max-Planck Institut für Astronomie and the Instituto de Astrofísica de Andalucía (CSIC). This research has made the use of the SIMBAAD data base, operated at ADC, Strasbourg, France.

REFERENCES

Barden, S. C. 1985, ApJ, 295, 162

Barker, L., & Hollenbach, R. 1972, J. Appl. Phys. 43, 4669

Barnes, T. G., Moffett, T. J., & Slovak, M. H. 1986, PASP, 98, 223

Beckers, J.M., & Brown T.M., 1978, Osser. Mem. Astrophys. Obs. Arcetri. No. 106, 189

Cochran, W. D., et al. 2004, ApJ, 611, L133

Duncan, D. K, et al. 1991, ApJS, 76, 383

Eaton, J. A., Henry, G. W., & Fekel, F. C. 2003, in The Future of Small Telescopes in the New Millennium, Volume II - The Telescopes We Use, ed. T. D. Oswalt (Dordrecht: Kluwer), 189

Erskine, D.J., & Ge, J. 2000, in Imaging the Universe in Three Dimensions: Astrophysics with Advanced Multi-Wavelength Imaging Devices, Proceedings from APS Conference Series 195, edited by W. van Breugel & J. Blland-Hawthorn, p. 501

Erskine, D.J.,2003, PASP, 115, 255

ESA. 1997, The *Hipparcos* and Tycho Cataloques (ESA SP-1200; Noordwijk: ESA)

Favata, F., Barbera, M., Micela, G., Sciortino, S. 1993, A&A, 277, 428

Fekel, F.C. 1997, PASP, 109, 514

Fischer, D. A., & Valenti, J. A. 2005, ApJ, 622, 1102

Ford, E.B. 2005, AJ, 129, 1706.

Ford, E.B. 2006, AJ, submitted [astro-ph/0412703].

Ge, J. 2002, ApJ, 571, L165

Ge, J., Erskine, D.J., & Rushford, M., 2002, PASP, 114, 1016

Ge, J., Mahadevan, S., van Eyken, J.C., DeWitt, C., Friedman, J., & Ren, D. 2004, Proc. SPIE, 5492, 711

Ge, J., et al. 2005, in Protostars and Planets V, Proceedings of the Conference held October 24-28, 2005, in Hilton Waikoloa Village, Hawaii. LPI Contribution No. 1286., 8410

Gelman, A., Carlin, J., Stern, H., and Rubin, D. Bayesian data analysis, Chapman & Hall, London, 1995.

Gonzalez, G. 1997, MNRAS, 285, 403

Gorskii, S. M., & Lebedev, V.P., 1977, Izv. Krym. Astrofiz. Obs. 57, 2281016

Gray, D. F. 1992, The observation and analysis of stellar photospheres, 2nd ed. (Cambridge University Press)

Gray, R. O., et al. 2003, AJ, 126, 2048

Gunn, J.E., et al. 2006, AJ, in press

Hall, J. C. 1996, PASP, 108, 313

Harvey, J. et al. 1995, in GONG'94: Helio-and Astro-Seismology from Earth and Space, Proceedings from APS Conference Series 76, edited by R.K. Ulrich, E.J. Rhodes, Jr., & W. Deppen, p. 432

Henry, G. W. 1999, PASP, 111, 845

Henry, G. W., Fekel, F. C., & Hall, D. S. 1995, AJ, 110, 2926

Henry, G. W., Baliunas, S. L., Donahue, R. A., Fekel, F. C., & Soon, W. 2000a, ApJ, 531, 415

Henry, G. W., Marcy, G. W., Butler, R. P., & Vogt, S. S. 2000b, ApJ, 529, L41

Høg, E., Fabricius, C., Makarov, V. V., et al. 2000, A&A, 355, L27

Jefferys, W. H., Fitzpatrick, M., J., & McArthur, B. E. 1987, Celestial Mechanics, 41, 39

Kozhevatov, I.E. 1983, Isseledovanie Geo.Aero.Fiz. Solusta No. 64, 42

Lomb, N.R., 1976, Ap&SS, 39, 447

Marcy, G., Butler, R. P., Williams, E., Bildsten, L., Graham, J. R., Ghez, A. M., & Garrett, J. J. 1997, ApJ, 481, 926

Marcy, G., Butler, R.P., Fischer, D., Vogt, S., Wright, J.T., Tinney, C.G., & Jones, R.A., 2005, Progress in Theoretical Physics Supplement No. 158, in press

Martinez Fiorenzano, A.F., Gratton, R.G., Desidera, S., Cosentino, R., & Endl, M. 2006, A&A, 442, 775

Mayor, M., & Queloz, D. 1995, Nature, 378, 355

McArthur, B., Jeffferys, W., & McCartney, J. 1994, Bull. A. A. S, 26, 900

Montes, D., Fernández-Figueroa, M. J., De Castro, E., Cornide, M., Latorre, A., & Sanz-Forcada J. 2000, A&AS, 146, 103

Montes, D., López-Santiago, J., Gálvez, M.C., Fernández-Figueroa, M.J., De Castro, E., & Cornide, M. 2001, MNRAS, 328, 45

Montes et al. 2001, A&A, 379, 976

Noyes, R.W., Hartmann, L.W., Baliunas, S.L., Duncan, D.K. & Vaughan, A.H. 1984, ApJ, 279, 763

Paulson, D. B., Saar, S. H., Cochran, W. D., & Henry, G. W. 2004, ApJ, 127, 1644

Pepe, F., et al. 2002, The Messenger, 110, 9

Pfeiffer, M. J., Frank, C., Baumueller, D., et al. 1998, A&AS, 130, 381

Queloz, D., Henry, G. W., Sivan, J. P., Baliunas, S. L., Beuzit, J. L., Donahue, R. A., Mayor, M., Naef, D., Perrier, C., & Udry, S. 2001, A&A, 379, 279

Ramsey. L.W., et al. 2006, PASP, in preparation

Reid, I.N. 2002, PASP, 114, 306

Saffe, C., Gómez, M., & Chavero, C. 2005, A&A, 443, 609

Santos, N.C. et al. 2000, A&A, 361, 265

Santos, N. C., Israelian, G., & Mayor, M., A&A, 2004, 415, 1153

Sato, B., Fischer, D. A., Henry, G. W., et al. 2005, ApJ, 633, 465

Scargle, J.D. 1982, ApJ, 263, 835

Soderblom, D. R., Oey, M. S., Johnson, D. R. H., Stone, R. P. S. 1990, AJ, 99, 595

Soderblom D. R., Duncan D. K., Johnson D. R. H., 1991, ApJ, 375, 722

Soderblom, D.R., et al., 1993, AJ, 105, 2299

Stumpff, P., 1980, A&AS, 41, 1

Strassmeier, K., Washuettl, A.; Granzer, Th., Scheck, M., & Weber, M. 2000, A&AS, 142, 275

Tonry, J., & Davis, M. 1979, AJ, 84 1511

VandenBerg, D.A., & Clem, J.L. 2003, AJ, 126, 778

Valenti, J.A., & Fischer, D.A. 2005, ApJS, 159, 141

van Eyken, J., Ge, J., Mahadvan, S., & DeWitt, C. 2004a, ApJ, 600, 79

van Eyken, J., et al. 2004b, Proc. SPIE, 5492, 445

Wolszczan, A., and Frail, D.A., 1992, Nature, 355, 145

York, D. G., et al. 2000, 120, 1579

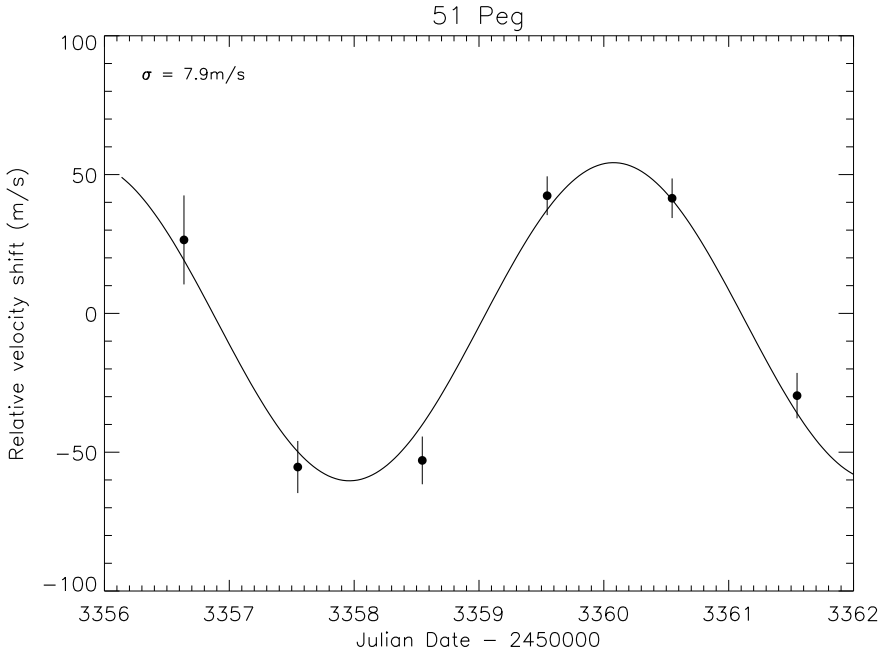

Fig. 1.— RV measurements of 51 Peg taken with ET at the 0.9 m coudé feed in 2005 May. The solid line is the predicted RV curve based on the orbital solution in Marcy et al. (1997). The exposure times were 15 minutes and the typical RV error for each point is 7.9 m s^{-1}.

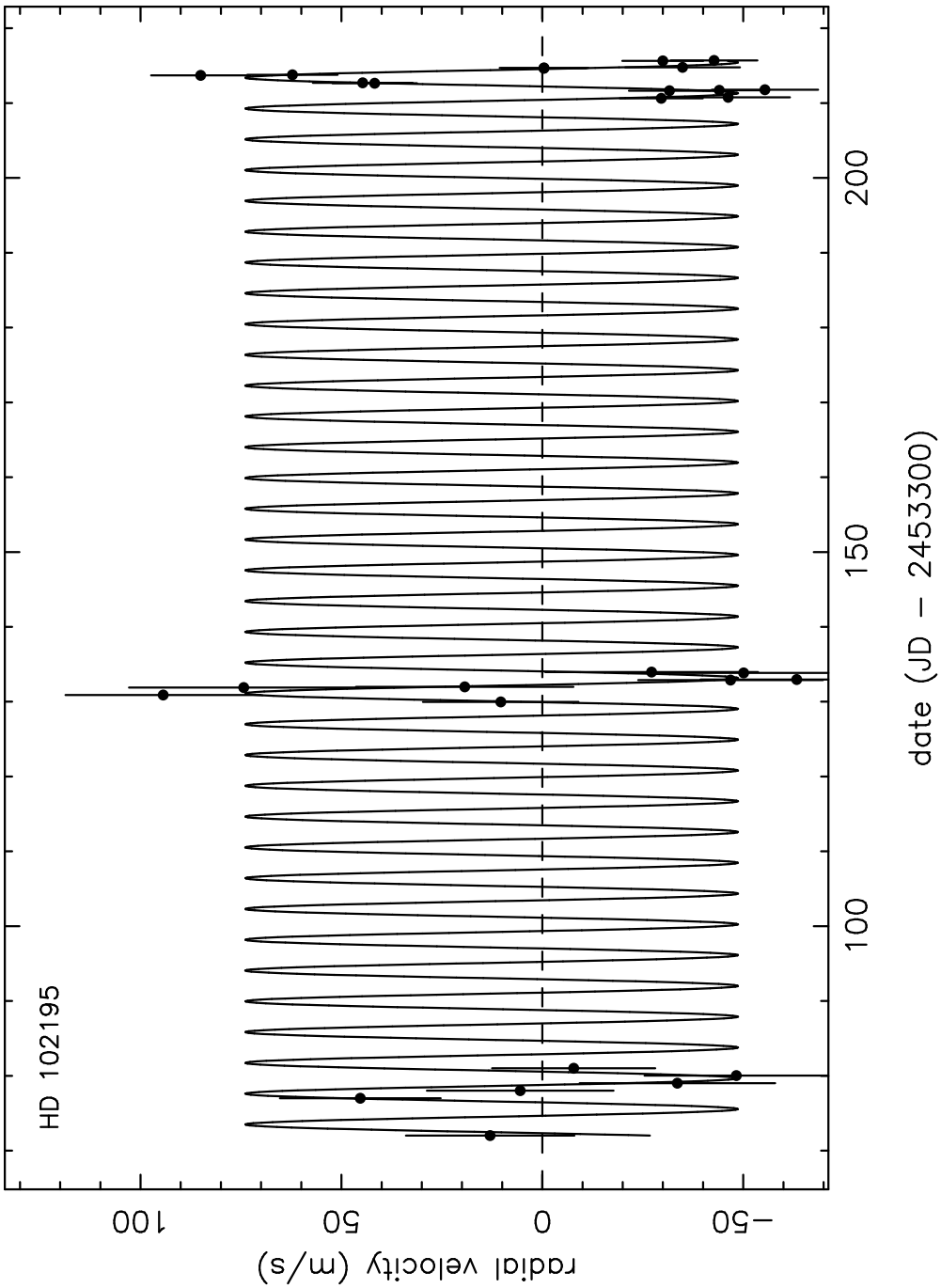

Fig. 2.— Radial velocities for HD 102195, showing the 28 measurements from ET at the KPNO coudé feed/2.1 m in the spring of 2005. The rms errors for the ET measurements at KPNO are ∼10 m s^{-1} and ∼20 m s^{-1} for the 2.1 m and coudé feed, respectively. The solid line is the Keplerian orbital fit to the observed data.

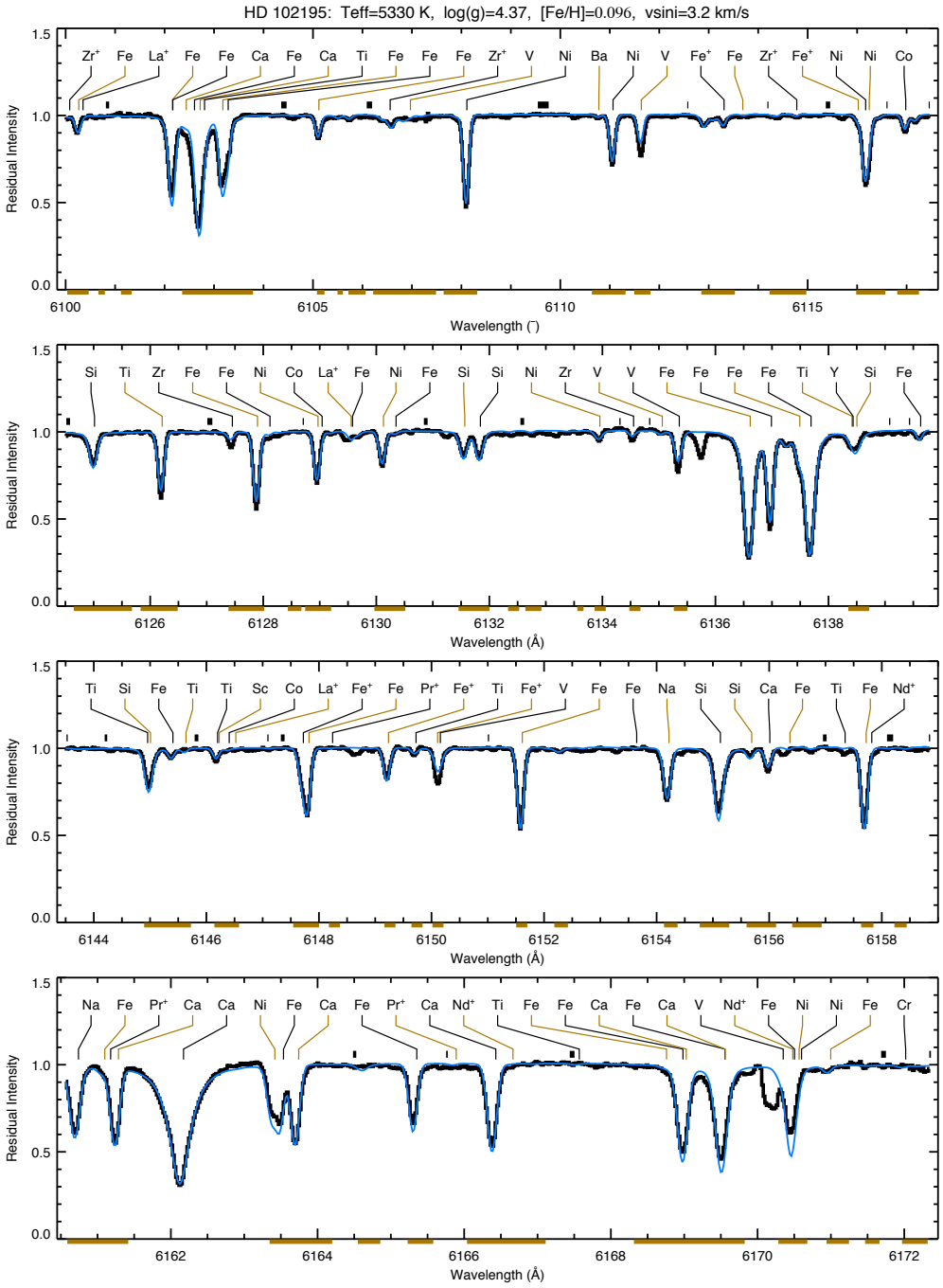

Fig. 3.— Part of the combined normalized observed spectrum and superimposed synthetic spectrum of HD 102195 for four different wavelength intervals. The black color lines are the observed data. The grey lines are the synthetic. The spectral resolution is $R = 150,000$ ($\sim$0.02 Å per pixel) and an average S/N $\sim$ 300 per pixel in the combined continuum spectrum. The synthetic spectrum is produced by a model using the stellar parameters in Table 3.

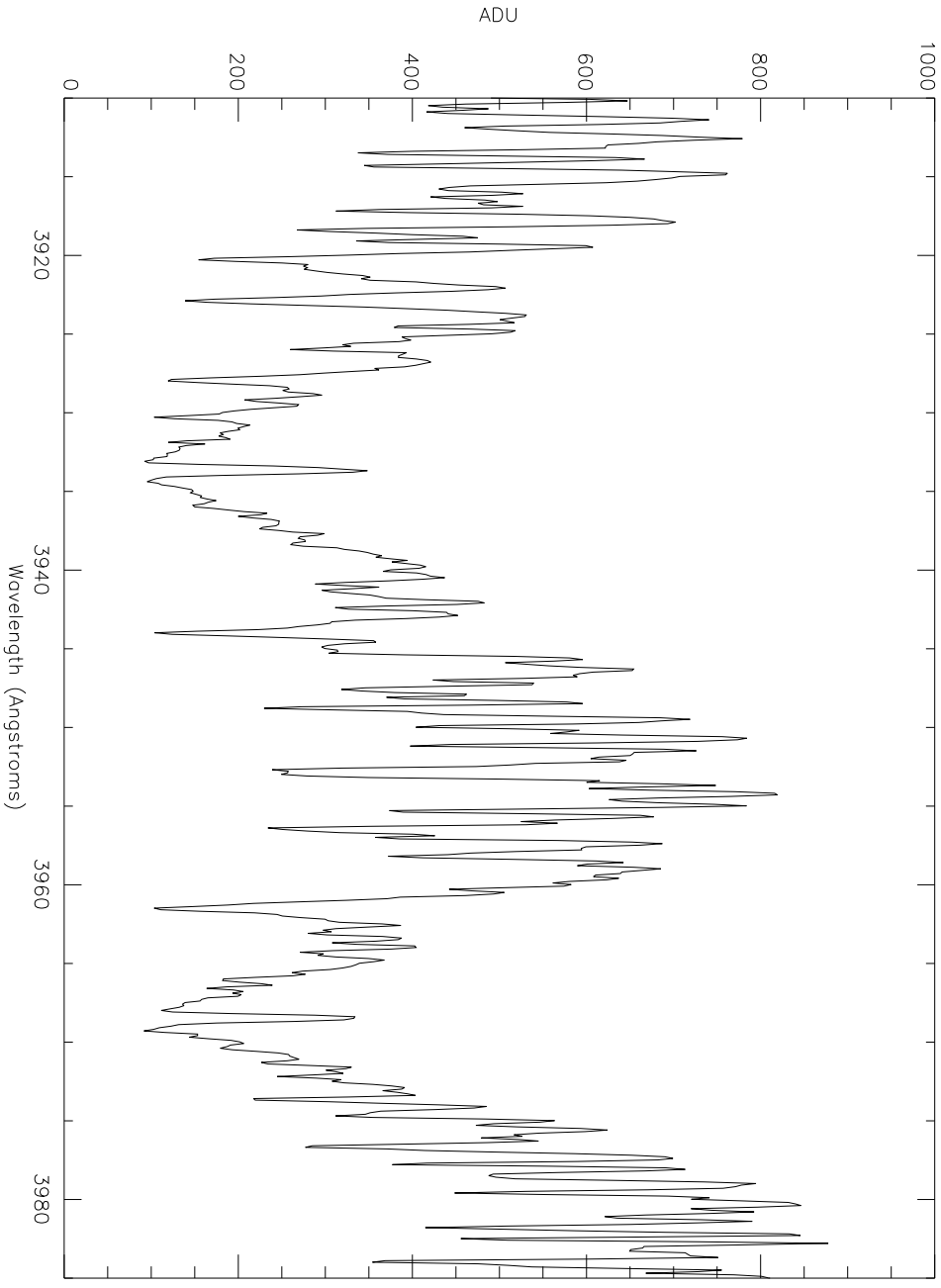

Fig. 4.— A typical Ca II H and K emission line spectrum of HD 102195 taken with the KPNO 0.9 m coudé long-slit spectrograph after the background is subtracted and the flux is summed. The spectral resolution is $R = 10,000$. H and K emission lines are clearly visible in the core of the broad H and K absorption lines.

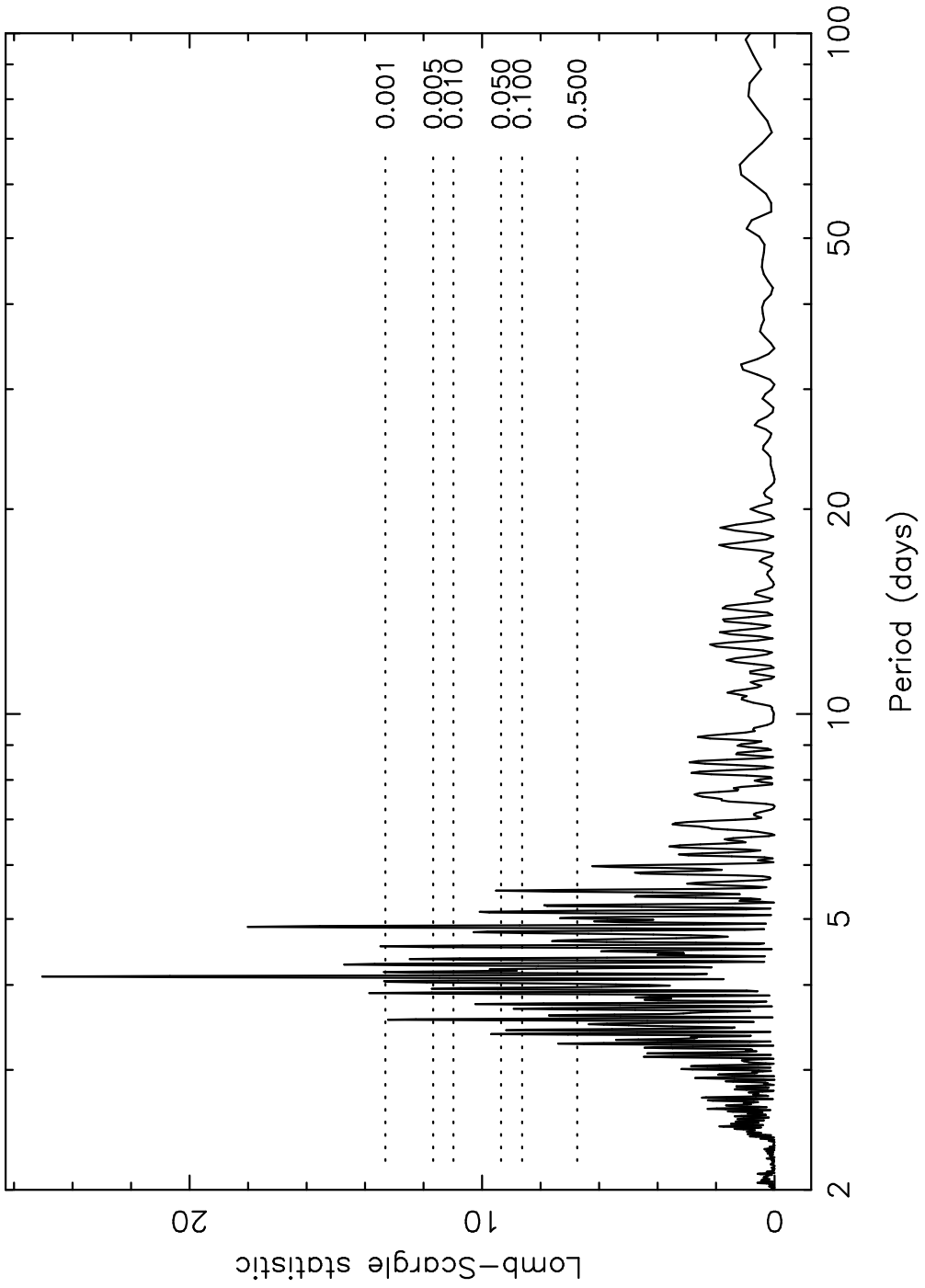

Fig. 5.— Periodogram of the velocities for HD 102195, showing peak power at 4.11 days with a false alarm probability $\sim 10^{-6}$.

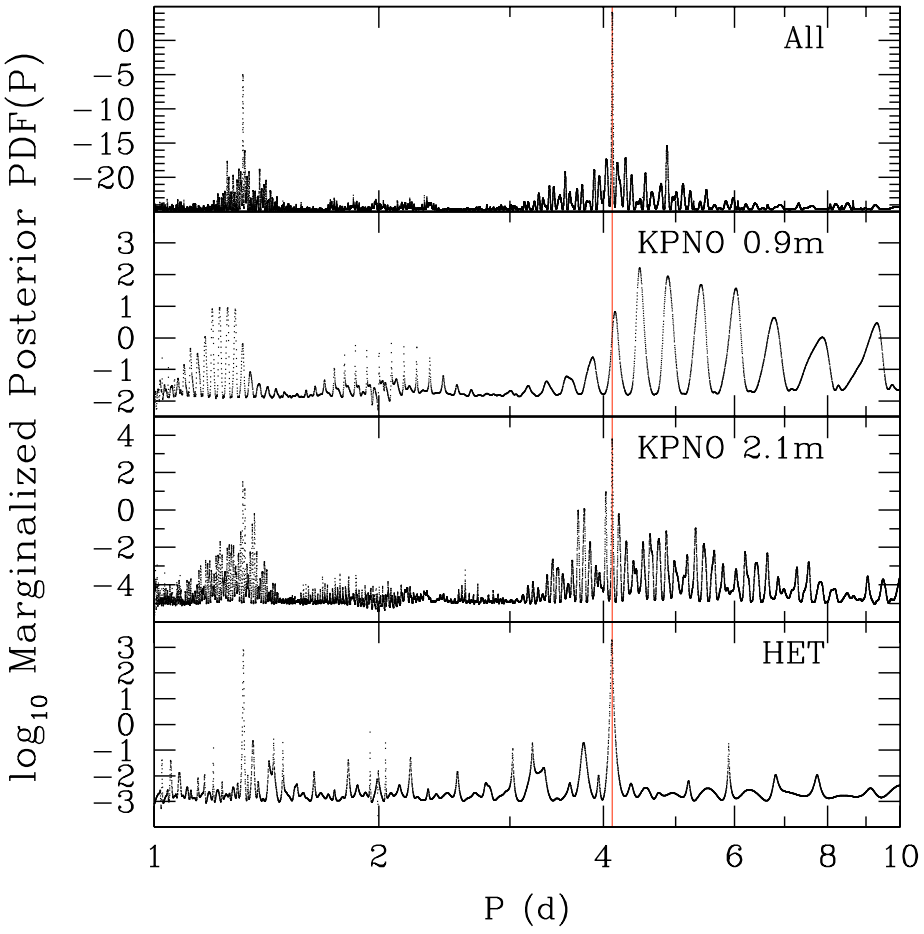

Fig. 6.— The posterior probability density function marginalized over all model parameters except for the orbital period for RV data taken at different telescopes.

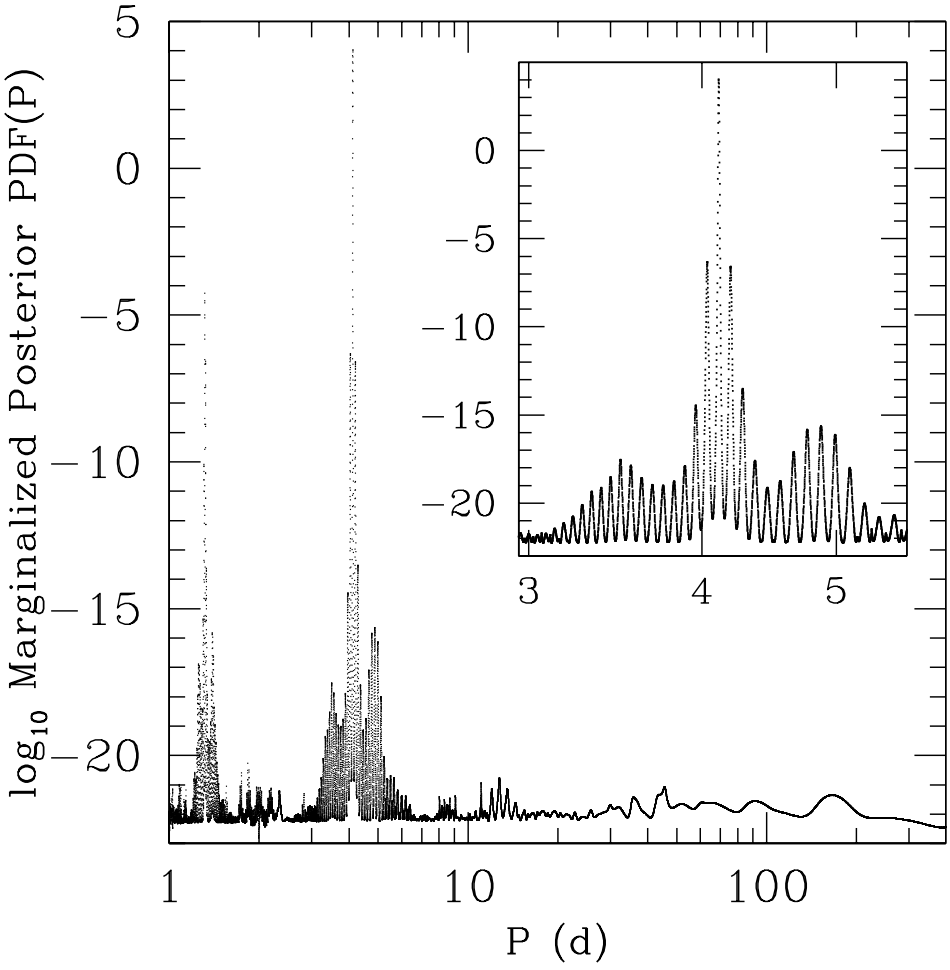

Fig. 7.— The marginalized posterior PDF combining all RV data taken at the coudé feed, 2.1 m and the HET. Nearly all of the power is in the 4.11-day period; there is no indication of any significant RV variation at the 12.3-day photometric period.

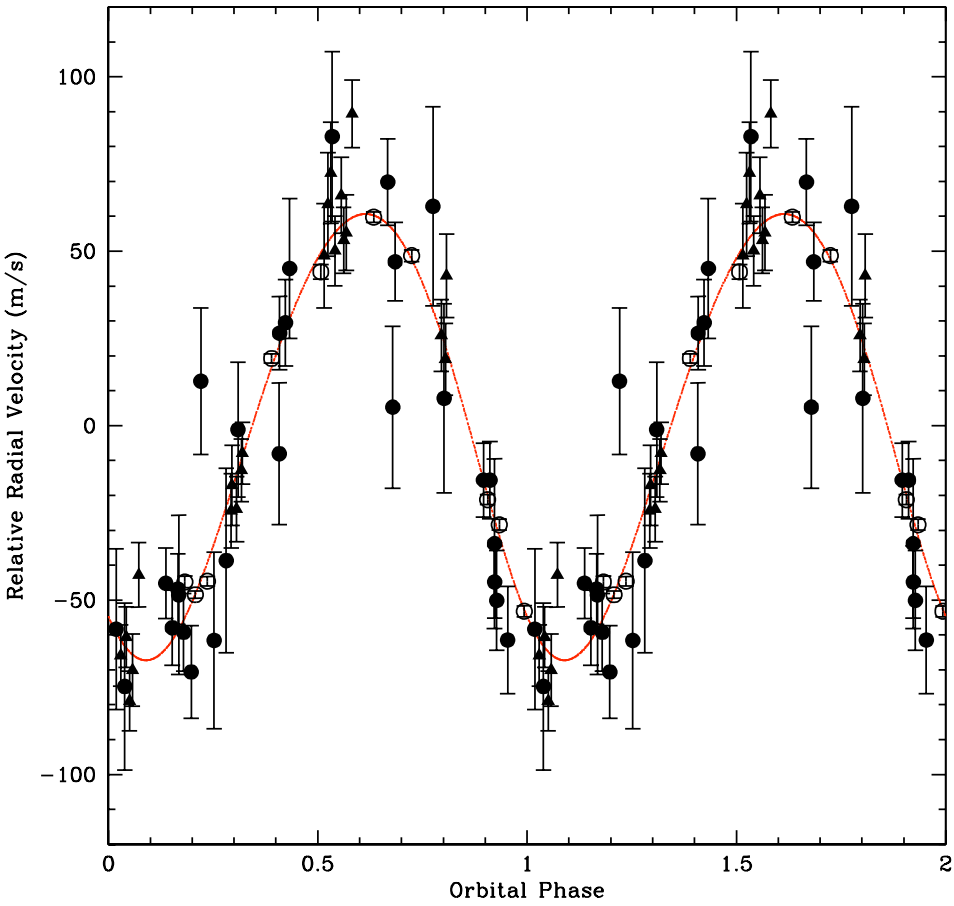

Fig. 8.— Phased radial velocities for HD 102195; the KPNO coudé data are filled circles, KPNO 2.1 m data are filled triangles, and the HET data are open circles. Two orbital cycles are shown and each observation is plotted as two points. The best fit to the data yields an orbital period of 4.11434 days and a velocity semiamplitude of 63.4 m s^{-1}. If the stellar mass is $0.93 M_{\odot}$, the derived minimum planetary mass is 0.488 M_J and the minimum orbital radius is 0.0491 AU.

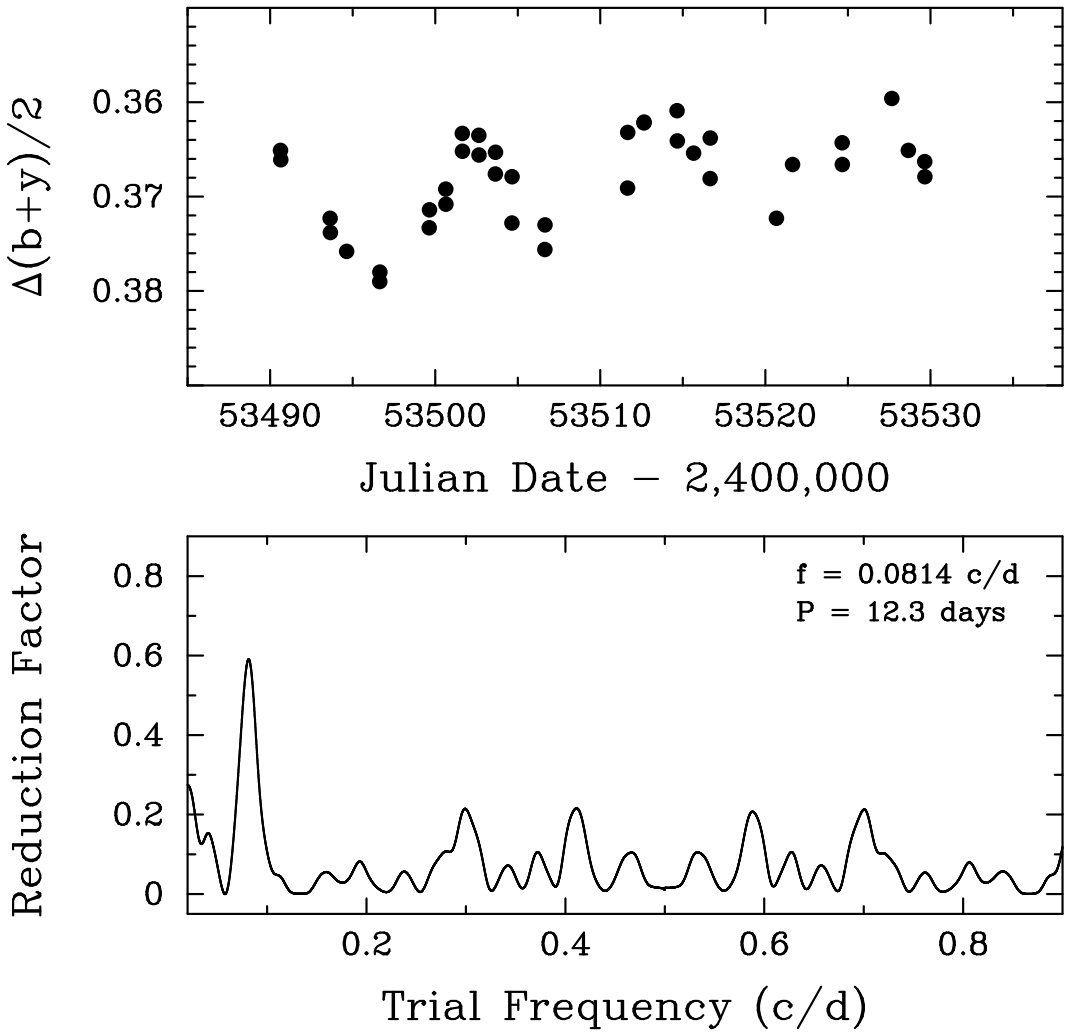

Fig. 9.— *Top*: The Strömgren $(b+y)/2$ photometric observations of HD 102195 obtained at the end of the 2004–05 observing season with the T10 0.8 m APT at Fairborn Observatory. A cyclic variation of about 0.015 mag in the brightness of the star is easily seen. *Bottom*: The power spectrum of the observations in the top panel. A clear period of 12.3 days is interpreted as the rotation period of the star.

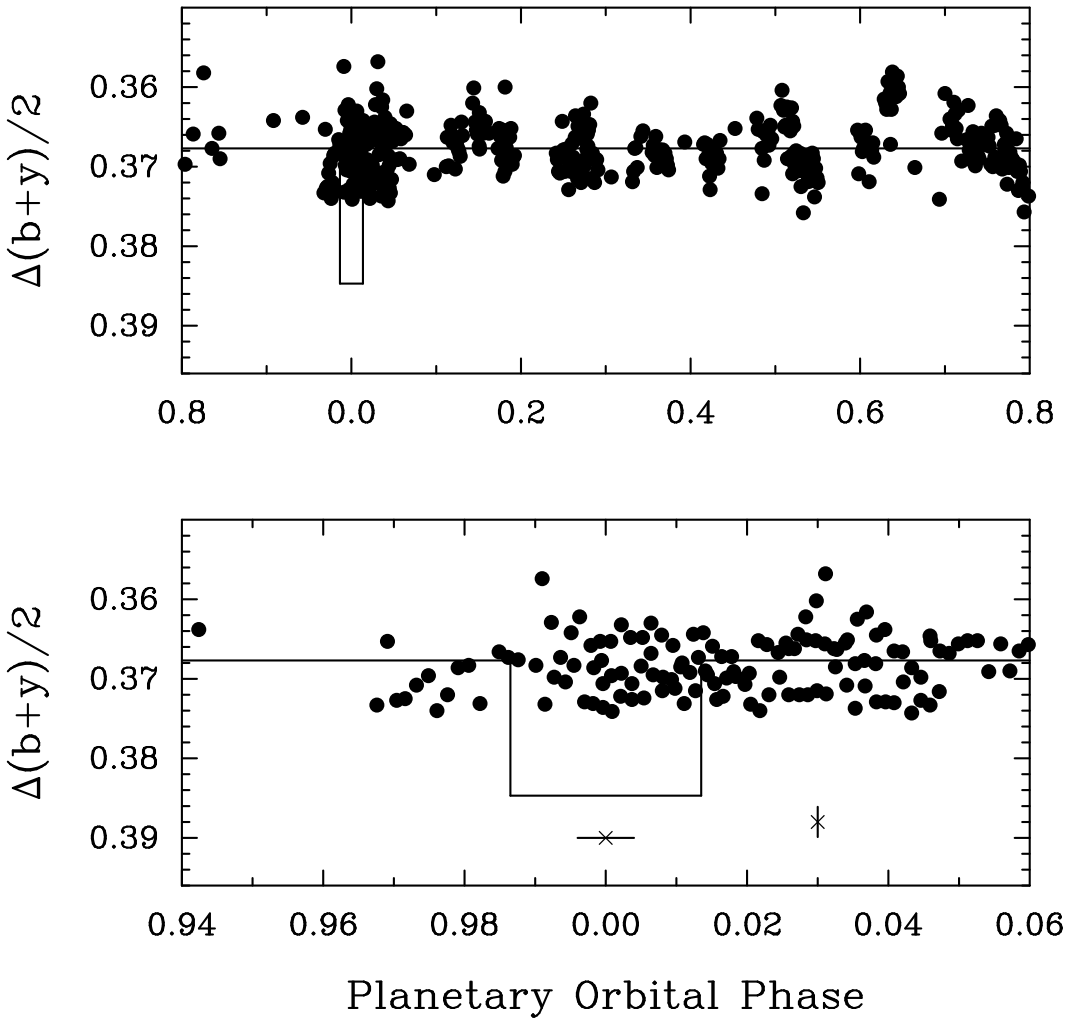

Fig. 10.— *Top*: The Strömgren $(b + y)/2$ photometric observations of HD 102195 obtained during the 2005–06 observing season with the T10 0.8 m APT at Fairborn Observatory and plotted against orbital phase of the planetary companion. The predicted time, depth, and duration of possible transits are shown schematically. The star exhibits no optical variability on the radial velocity period larger than 0.0004 mag or so. *Bottom*: The observations around the predicted time of transit are replotted with an expanded scale on the abscissa. The error bars are described in the text. Even very shallow transits are ruled out by these observations.

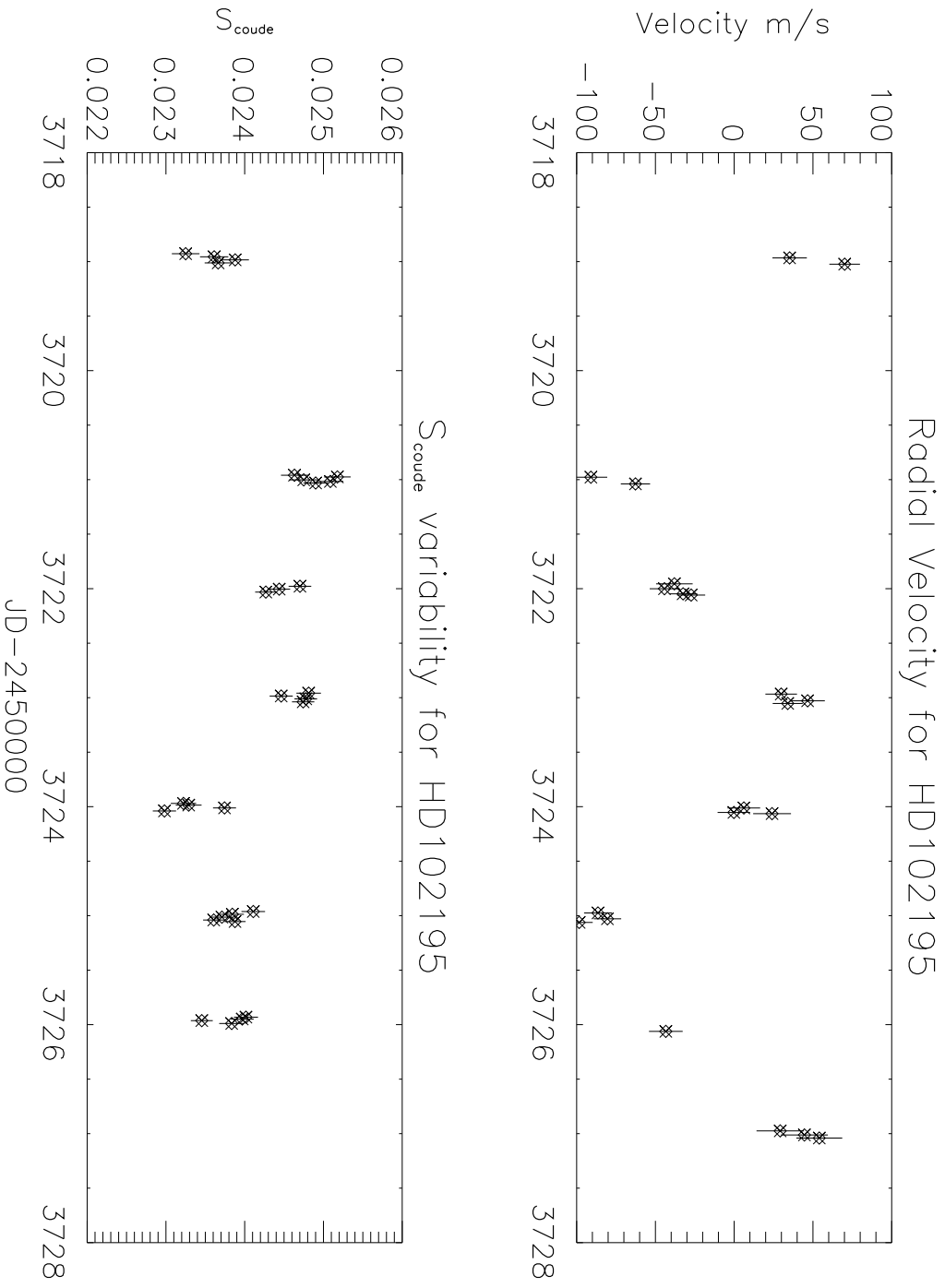

Fig. 11.— The measurements of the S_{coude} index (*bottom*) and RV (*top*) during the same observation run at Kitt Peak.

Table 1. Radial Velocities for HD 102195

JD −2450000	Instrument[a]	RV m s^{-1}	errors m s^{-1}	JD −2450000	Instrument[a]	RV m s^{-1}	errors m s^{-1}
3372.014	CF, BK2	133.0	21.0	3696.034	HET	−60.6	1.3
3376.999	CF, BK2	165.3	20.0	3697.034	HET	−52.0	1.1
3378.011	CF, BK2	125.5	23.2	3701.029	HET	−55.9	0.8
3379.013	CF, BK2	86.4	24.3	3704.016	HET	−35.8	1.3
3380.024	CF, BK2	71.7	22.8	3718.966	2.1m	56.0	10.9
3381.011	CF, BK2	112.2	20.3	3719.023	2.1m	90.0	9.7
3429.966	CF, BK4	−99.6	19.3	3720.978	2.1m	−69.5	10.3
3430.892	CF, BK4	−15.6	24.3	3721.039	2.1m	−42.1	9.2
3431.882	CF, BK4	−35.7	28.5	3721.956	2.1m	−16.5	11.5
3431.991	CF, BK4	−90.7	27.1	3722.001	2.1m	−23.3	9.3
3432.881	CF, BK4	−156.9	23.0	3722.048	2.1m	−12.2	9.0
3432.966	CF, BK4	−173.3	24.0	3722.059	2.1m	−7.2	8.9
3433.844	CF, BK4	−160.1	25.3	3722.967	2.1m	50.7	10.0
3433.963	CF, BK4	−137.2	26.5	3723.029	2.1m	66.6	10.9
3510.641	2.1m, BK5	−29.6	10.3	3723.053	2.1m	53.7	9.5
3510.769	2.1m, BK5	−46.2	15.4	3724.012	2.1m	26.5	10.3
3511.643	2.1m, BK5	−31.6	10.1	3724.053	2.1m	19.6	10.3
3511.699	2.1m, BK5	−44.0	11.1	3724.064	2.1m	43.6	11.9
3511.774	2.1m, BK5	−55.4	13.2	3724.975	2.1m	−65.3	8.8
3512.641	2.1m, BK5	41.7	10.5	3725.029	2.1m	−60.0	8.7
3512.699	2.1m, BK5	44.7	12.4	3725.062	2.1m	−78.3	8.6
3513.704	2.1m, BK5	85.0	12.3	3726.062	2.1m	−23.8	10.6
3513.777	2.1m, BK5	62.2	11.2	3726.975	2.1m	49.3	14.9
3514.646	2.1m, BK5	−0.4	10.6	3727.012	2.1m	64.1	14.8
3514.708	2.1m, BK5	−0.4	11.0	3727.040	2.1m	73.1	14.5
3514.775	2.1m, BK5	−34.9	14.3	3731.949	HET	41.3	1.4
3515.638	2.1m, BK5	−30.0	10.1	3737.946	HET	−52.2	1.3
3515.700	2.1m, BK5	−42.7	10.8	3740.922	HET	−28.6	1.1
3694.035	HET	36.7	1.8	3742.912	HET	11.9	1.1
				3743.915	HET	52.3	1.1

[a] CF = 0.9-m Coude Feed; BK = Block

Table 2. PHOTOMETRIC OBSERVATIONS OF HD 102195

Observation Date (HJD − 2,400,000)	$\Delta(b+y)/2$ (mag)
53,490.6339	0.3651
53,490.6494	0.3661
53,493.6380	0.3723
53,493.6498	0.3738
53,494.6381	0.3758

Note. — Table 2 is presented in its entirety in the electronic edition of the Astrophysical Journal. A portion is shown here for guidance regarding its form and content.

Table 3. Stellar Parameters for HD 102195

Parameter	Value
V	8.05
M_V	5.73
$B-V$	0.84
Spectral type	G8V
Distance	29 pc
[Fe/H]	0.096 ± 0.032
$T_{\rm eff}$	5330 ± 28 K
$v \sin i$	3.23±0.07 km s^{-1}
$\log g$	4.368±0.038 [log(cm s^{-2})]
BC	−0.177
$L_{\rm star}$	0.463±0.034 L$_\odot$
$M_{\rm star}$	0.926±0.016 $M_\odot$
$R_{\rm star}$	0.835±0.016 $R_\odot$
$\log R'_{HK}$	−4.30
$P_{\rm rot}$	12.3±0.2 days
Age	0.6-4.2 Gyr

Table 4. Equivalent width (EW) and surface flux ($\log F_S$) of the different chromospheric activity indicators

Date	EW(Å) in the subtracted spectrum						$\log F_S$ (erg cm^{-2} s^{-1})					
	Ca II			Ca IIIRT			Ca II			Ca II IRT		
	K	H	Hα	λ8498	λ8542	λ8662	K	H	Hα	λ8498	λ8542	λ8662
01/14/06	0.313	0.164	0.045	0.084	0.126	0.122	5.75	6.04	5. 29	5.43	5.61	5.59

Table 5. Orbital Parameters for HD 102195b

Parameter	Value
P	4.11434±0.00089 days
T_p	2453732.7±0.5
e	<0.14
a	0.0491 AU
ω (deg)	143.4±15.4
K	63.4±2.0 m s^{-1}
$m \sin i$	0.488 ± 0.015 $M_J \frac{M_*}{0.93 M_\odot}$
σ_j	5.8±1.8 m s^{-1}
rms	16.0 m s^{-1}